Rapid Communications

Coulomb shift in the mirror pair of ^{14}C and ^{14}O as a signature of the linear-chain structure

T. Baba[1] and M. Kimura[1,2]
[1]*Department of Physics, Hokkaido University, 060-0810 Sapporo, Japan*
[2]*Reaction Nuclear Data Centre, Faculty of Science, Hokkaido University, 060-0810 Sapporo, Japan*

(Received 16 October 2018; revised manuscript received 3 January 2019; published 13 February 2019)

Coulomb shifts of the linear-chain states are theoretically investigated for the mirror pair of ^{14}C and ^{14}O by using the antisymmetrized molecular dynamics. Energy shift of the σ-bond linear-chain states is found and it is due to the reduction in the Coulomb energy associated with the spatially extended σ orbit. This new signature supports the existence of the linear-chain formation and encourages further experimental investigations.

DOI: 10.1103/PhysRevC.99.021303

Introduction. The linear-chain structure is an interesting topic in nuclear physics and this novel cluster structure can provide us with an understanding of the nature of the exotic nuclear formation. The linear-chain states in neutron-rich carbon isotopes have been focused on [1–21] because the valence neutrons play a glue-like role to stabilize extreme shapes. This role is well known as the molecular orbits in beryllium isotopes [22–24] and they are classified into two types: the π orbit which is perpendicular to the z axis of the 2α core, and the σ orbit which is parallel to the z axis. The molecular-orbital picture was extended to the linear-chain states in carbon isotopes [2]. For ^{14}C, Suhara *et al.* predicted the π-bond linear-chain band by using antisymmetrized molecular dynamics (AMD) [7,8]. The energies, moments of inertia, and α-decay widths of the resonances observed by the $\alpha + {}^{10}$Be elastic scattering [9,13,17] reasonably agree with the predicted π-bond linear chain. Therefore, the π-bond linear-chain formation is likely to exist in ^{14}C. In addition to the π-bond linear chain, we suggested the σ-bond linear-chain formation [16,19]. It was predicted that the σ-bond linear chain should have different a decay pattern from that of the π-bond linear chain. The resonances observed by the ^{9}Be(^{9}Be, $\alpha + {}^{10}$Be)α reaction [14,18] looks to be a promising candidate for the σ-bond linear-chain configuration.

To establish the existence of the linear-chain structure, we need more evidences and we focus on the Coulomb shift in the mirror pair of ^{14}C-^{14}O. Due to charge symmetry of nuclear interaction, the spectroscopic properties of mirror nuclei should be quite similar. However, the large difference in the excitation energies of the $s_{1/2}$ levels exists in the nucleus with the loosely bound proton and its mirror nucleus. It is due to the reduction of the Coulomb energy associated with the spatially extended s-wave, which is known as the Thomas-Ehrman shift [25–30]. The Thomas-Ehrman shift can be extended to the cluster structure based on the molecular-orbital picture of Be isotopes because the σ orbit is composed of the s-wave and d-wave. In fact, the Coulomb shifts of the ^{10}Be and ^{10}C was discussed from the viewpoint of the molecular-orbital picture [31]. In this previous work, the Coulomb shift is prominent for the 0^+_1 state with the π-orbit nucleons which is dominated by the p-wave. On the other hand, the Coulomb shift of the 0^+_2 state with the σ orbit is rather smaller than the 0^+_1 state. This reduction is due to the spatially extended σ orbit which dominated by the s-wave and enhances the α-α clustering.

In this work we extend the discussion to the linear chain of ^{14}C-^{14}O. In particular, we expect a large Thomas-Ehrman shift in the σ-bond linear chain because of its much larger spatial extent. However, the σ orbit of ^{14}C-^{14}O does not have the s wave but rather, the pf wave. Therefore, it is not clear that the σ-bond linear chain of ^{14}C-^{14}O shows the Thomas-Ehrman shift. Thus, we investigate Coulomb shifts of the linear-chain states in ^{14}C and ^{14}O based on the AMD calculation. In particular, we focus on single-particle properties of the molecular orbits to clarify the origin of large energy shifts in the σ-bond linear chain. In addition, we predict the α-decay widths of the linear-chain states in ^{14}O.

Theoretical framework. In the AMD framework, the microscopic A-body Hamiltonian used in this work reads

$$\hat{H} = \sum_{i=1}^{A} \hat{t}_i - \hat{t}_{\rm c.m.} + \sum_{i<j}^{A} \hat{v}^N_{ij} + \sum_{i<j}^{Z} \hat{v}^C_{ij} \tag{1}$$

$$= \hat{H}^{\rm sym} + \hat{v}^C, \tag{2}$$

where Gogny D1S [32] is used as the effective nucleon-nucleon interaction. The $\hat{t}_{\rm c.m.}$ is kinetic energy of the center of mass. We separate the Coulomb interaction part $\hat{v}^C$ from the isospin symmetric part $\hat{H}^{\rm sym}$. The Coulomb interaction $\hat{v}^C$ is approximated by a sum of seven Gaussians. The Gaussian form cannot exactly reproduce a long-range part of the Coulomb force. Although it is not easy to calculate the exact values in this method due to the computational cost, we deduce that its effect is very small, on the order of 10 keV, because we checked it for the p shell in the lighter nucleus.

The AMD wave function $\Phi_{\rm AMD}$ is represented by a Slater determinant of single-particle wave packets,

$$\Phi_{\rm AMD} = \mathcal{A}\{\varphi_1, \varphi_2, \ldots, \varphi_A\} = \frac{1}{\sqrt{A!}} \det[\varphi_i(\boldsymbol{r}_j)]. \tag{3}$$

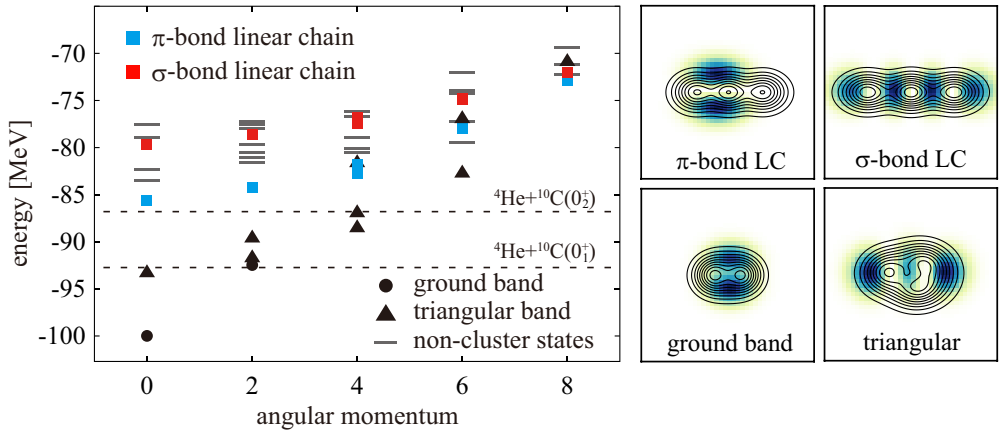

FIG. 1. Left: Positive-parity energy levels of ^{14}O up to $J^\pi = 8^+$. The filled circles, triangles, and boxes show the ground, triangular, and linear-chain bands, while lines show the noncluster states. Dashed lines show theoretical threshold energies. Right: Density distributions of intrinsic wave functions in ^{14}O. Contour lines show the neutron density distribution and blue plots show the single-particle orbit occupied by the most weakly bound proton.

Here, φ_i is the single-particle wave packet which is a direct product of the deformed Gaussian spatial part [33], spin (χ_i) and isospin (ξ_i) parts,

$$\varphi_i(\boldsymbol{r}) = \phi_i(\boldsymbol{r}) \otimes \chi_i \otimes \xi_i, \tag{4}$$

$$\phi_i(\boldsymbol{r}) = \prod_{\sigma=x,y,z} \left(\frac{2\nu_\sigma}{\pi}\right)^{1/4} \exp\left\{-\nu_\sigma\left(r_\sigma - \frac{Z_{i\sigma}}{\sqrt{\nu_\sigma}}\right)^2\right\},$$

$$\chi_i = a_i\chi_\uparrow + b_i\chi_\downarrow, \quad \xi_i = \text{proton or neutron}. \tag{5}$$

The centroids of the Gaussian wave packets $\boldsymbol{Z}_i$, the direction of nucleon spin a_i, b_i, and the width parameter of the deformed Gaussian ν_σ are the variables determined by the frictional cooling method [34]. In this study, we add the constraint potential with respect to the quadrupole deformation parameter β.

After the variational calculation, the eigenstate of the total angular momentum J is projected out. In addition, we perform the generator coordinate method [35] by employing the quadrupole deformation parameter β as the generator coordinate. The details of the angular momentum projection and the generator coordinate method (GCM) are given in our previous work [11]. Using the GCM wave functions Ψ_n, we calculate the energy which can be divided into the Coulomb energy component and other components from Eq. (2),

$$E_n = \langle\Psi_n|\hat{H}|\Psi_n\rangle = \langle\hat{H}_n^{\rm sym}\rangle + \langle\hat{v}_n^C\rangle, \tag{6}$$

$$\langle\hat{H}_n^{\rm sym}\rangle = \langle\Psi_n|\hat{H}^{\rm sym}|\Psi_n\rangle, \tag{7}$$

$$\langle\hat{v}_n^C\rangle = \langle\Psi_n|\hat{v}^C|\Psi_n\rangle. \tag{8}$$

To investigate the properties of the valence neutrons around the core nucleus, we calculate the neutron single-particle orbits $\widetilde{\phi}_s$ of the intrinsic wave function. The details of this calculation are given in our previous work [11]. To discuss the origin of the Coulomb shift, we also calculate the root-mean-square radius of the single-particle orbit,

$$\sqrt{\langle r^2_{\rm s.p.}\rangle} = \sqrt{\langle\widetilde{\phi}_s|\hat{r}^2|\widetilde{\phi}_s\rangle}, \tag{9}$$

and the single-particle Coulomb energy,

$$\langle\hat{v}^C_{\rm s.p.}\rangle = \langle\widetilde{\phi}_s|\hat{v}^C|\widetilde{\phi}_s\rangle, \tag{10}$$

We estimate the α-decay width from the reduced width amplitude (RWA) [21]. To calculate the RWA, we need the intrinsic wave functions for ^{10}Be, ^{10}C, and ^{4}He, and they are generated by the AMD energy variation. For ^{10}C (^{10}Be), we obtain two different intrinsic wave functions in which two valence protons (neutrons) occupy the so-called π- and σ orbits, respectively. We regard that the former correspond to the ground band (the 0^+_1 and 2^+_1 states), whereas the latter is the excited band (the 0^+_2 and 2^+_3 states). In the following calculations, we assume that the ^{4}He has always $j^\pi = 0^+$. In order to calculate the RWA, we employ the Laplace expansion method given in Ref. [36].

Results. Figure 1 shows the calculated energy levels of ^{14}O as a function of the angular momentum (left panel). These energy levels are classified into three cluster bands and noncluster states. The filled circles, triangles, and blue and red boxes show the ground, triangular, π-bond and σ-bond linear-chain bands, respectively. Each band is dominantly composed of the intrinsic wave function shown in density distributions (right panels). It is found that these bands correspond to the triangular, and π- and σ-bond linear-chain bands in ^{14}C discussed in our previous work [16]. To investigate the charge symmetry between ^{14}O and ^{14}C, we compare

TABLE I. Binding energies (MeV) and Coulomb energies (MeV) of the ground states in ^{14}C and ^{14}O.

	^{14}C	^{14}O	Difference
Binding energy	− 106.19	− 99.99	6.20
Coulomb energy	7.31	13.34	6.03

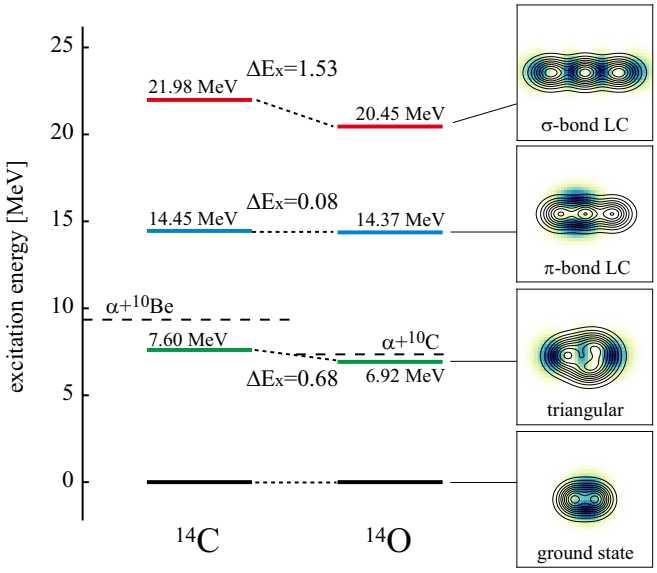

FIG. 2. Energy spectra for $J^\pi = 0^+$ of ^{14}C (left levels) and ^{14}O (right levels). Levels are marked by an excitation energy in units of MeV. Dashed lines show theoretical thresholds.

geometric properties of the linear-chain states with each other. For example, the rms radii of π- and σ-bond linear-chain states in ^{14}O(0^+) are 3.23 and 3.96 fm, which are almost same those in ^{14}C(0^+), 3.24 and 3.98 fm, respectively. In addition, the moment of inertia of the linear-chain bands in ^{14}O are $\hbar^2/2\mathscr{I} = 177$ keV for π-bond linear chains and 103 keV for σ-bond linear chains, respectively. They are very close to those of ^{14}C, $\hbar^2/2\mathscr{I} = 179$ and 105 keV. These suggest the good charge symmetry of the mirror pair of ^{14}C and ^{14}O. Binding energies and Coulomb energies of the ground states are listed in Table I.

Figure 2 shows the comparison of excitation energies between ^{14}C and ^{14}O for $J^\pi = 0^+$ states. The energy shift ΔE_x is defined as the difference of excitation energies,

$$\Delta E_x = \{E_n(^{14}\mathrm{C}^*) - E_{\mathrm{g.s.}}(^{14}\mathrm{C})\} - \{E_n(^{14}\mathrm{O}^*) - E_{\mathrm{g.s.}}(^{14}\mathrm{O})\}. \quad (11)$$

The energy shift of the σ-bond linear chain, $\Delta E_x = 1.53$ MeV, is much larger than those of the triangular-cluster configuration ($\Delta E_x = 0.68$ MeV) and the π-bond linear chain ($\Delta E_x = 0.08$ MeV). To discuss the origin of this large energy shift, we compare it with the Coulomb energy differences in Table II. If the mirror pair has the good charge symmetry,

$$\langle \hat{H}_n^{\mathrm{sym}} \rangle (^{14}\mathrm{C}) \approx \langle \hat{H}_n^{\mathrm{sym}} \rangle (^{14}\mathrm{O}), \quad (12)$$

then Eq. (11) is rewritten as

$$\begin{aligned}\Delta E_x &\approx \left\{ \langle \hat{v}_n^C \rangle (^{14}\mathrm{C}^*) - \langle \hat{v}_n^C \rangle (^{14}\mathrm{O}^*) \right\} \\ &\quad - \left\{ \langle \hat{v}_{\mathrm{g.s.}}^C \rangle (^{14}\mathrm{C}) - \langle \hat{v}_{\mathrm{g.s.}}^C \rangle (^{14}\mathrm{O}) \right\}, \\ &\equiv \Delta \langle \hat{v}_x^C \rangle . \end{aligned} \quad (13)$$

The Coulomb energy difference of the σ-bond linear chain, $\Delta \langle \hat{v}_x^C \rangle = 1.45$ MeV, is rather larger than those of other configurations. Note that this Coulomb energy difference is very close to the energy shift ($\Delta E_x = 1.53$ MeV). Therefore, we conclude that the large difference of the excitation energies in the σ-bond linear-chain dominantly comes from the Coulomb energy difference.

In general, it is difficult for the Gogny interaction to reproduce the size of an α particle. Thus, to discuss the dependence of the effective internucleon force we also check the energy shifts using Volkov No. 2 [37] ($m = 0.58$). Binding energies of the ground states are 106.66 MeV for ^{14}C and 99.64 MeV for ^{14}O. Energy shifts of the triangular-cluster, π-bond linear chain, and σ-bond linear chain states are $\Delta E_x = 0.99$, 0.83, and 1.88 MeV, respectively. Therefore, the large difference of the energy shift can be also seen in the only σ-bond linear-chain states in the case of Volkov No. 2. This result shows the independence of the effective internucleon force.

To get a deeper insight into the origin of the large Coulomb shift, we focus on single-particle properties listed in Table III. We roughly estimate the Coulomb energy induced from two valence protons in the σ orbit from Table III,

$$-2\left\{ \langle \hat{v}_{\mathrm{s.p.}}^C \rangle (\sigma) - \langle \hat{v}_{\mathrm{s.p.}}^C \rangle (\mathrm{g.s.}) \right\} = -2 \times (2.42 - 3.10) = 1.36, \quad (14)$$

which is also close to both the energy shift and the Coulomb energy difference, that is,

$$\Delta E_x \approx \Delta \langle \hat{v}_x^C \rangle \approx -2\left\{ \langle \hat{v}_{\mathrm{s.p.}}^C \rangle (\sigma) - \langle \hat{v}_{\mathrm{s.p.}}^C \rangle (g.s.) \right\}. \quad (15)$$

This reduction of the Coulomb energy of the σ orbit is derived from its large spatially extent. For example, the radius of the single particle of π orbit, 2.95 fm, is smaller than those of the ground state (3.11 fm) and triangular-cluster configuration (3.90 fm). In contrast, the radius of the single particle of the σ orbit is 4.85 fm, which is huge. Therefore, the large energy

TABLE II. Energy shifts ΔE_x (MeV) defined by Eq. (11) and Coulomb energy differences $\Delta \langle \hat{v}_x^C \rangle$ (MeV) defined by Eq. (13).

	0^+		2^+		4^+	
Band	ΔE_x	$\Delta \langle \hat{v}_x^C \rangle$	ΔE_x	$\Delta \langle \hat{v}_x^C \rangle$	ΔE_x	$\Delta \langle \hat{v}_x^C \rangle$
Ground	0	0	0.27	0.01		
Triangular (K=0)	0.68	0.72	0.85	0.73	1.04	0.83
Triangular (K=2)			0.85	0.76	1.09	0.77
π bond	0.08	0.59	0.24	0.63	1.04	0.00
					0.27	0.30
σ bond	1.53	1.45	1.31	1.04	1.49	0.34
					1.01	0.40

TABLE III. Single-particle energies (MeV), radii (fm), and Coulomb energies (MeV) of the most weakly bound neutron (for ^{14}C) or proton (for ^{14}O).

	ϵ		$\sqrt{\langle r_{\mathrm{s.p.}}^2 \rangle}$		$\langle \hat{v}_{\mathrm{s.p.}}^C \rangle$
	^{14}C	^{14}O	^{14}C	^{14}O	^{14}O
Ground state	−4.37	−1.82	3.12	3.11	3.10
Triangular	−5.32	−2.14	3.72	3.90	2.80
π bond	−6.95	−3.92	2.92	2.95	2.96
σ bond	−4.11	−1.76	4.85	4.85	2.42

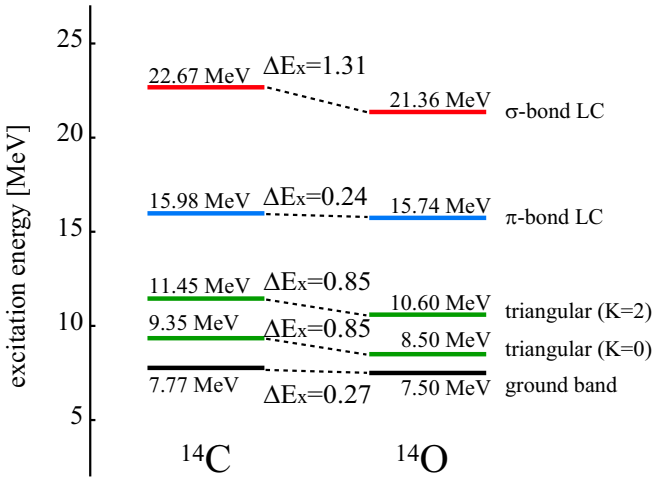

FIG. 3. Energy spectra for $J^\pi = 2^+$ of ^{14}C and ^{14}O.

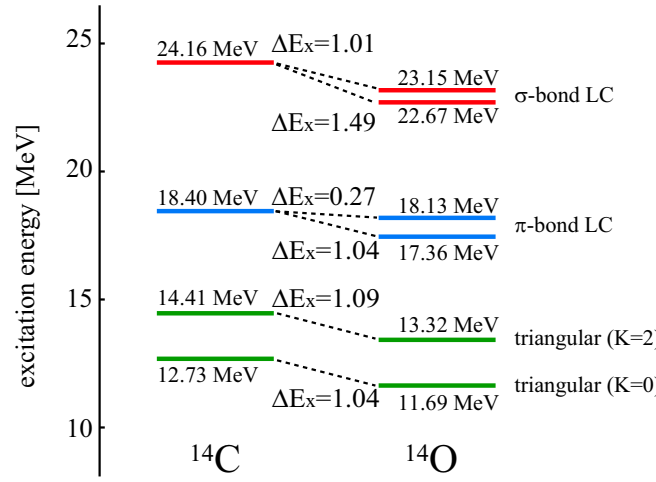

FIG. 4. Energy spectra for $J^\pi = 4^+$ of ^{14}C and ^{14}O.

difference of the σ-bond linear chain can be illustrated by the reduction in the Coulomb energy associated with the spatially extended σ orbit. Namely, we can see the Thomas-Ehrman shift in the σ-bond linear-chain states although the main component of the σ orbit is the pf orbit in the case of ^{14}C-^{14}O. The Thomas-Ehrman shift is also suggested in the pair of ^{10}Be-^{10}C [31]. In the mirror pair of ^{10}Be and ^{10}C, the energy difference of the σ-bond states is $\Delta E_x = 1.0$ MeV against the ground state, which is a bit smaller than that of ^{14}C-^{14}O. The radius of the single particle of the σ orbit in ^{10}Be-^{10}C must be smaller than that in ^{14}C-^{14}O. Therefore, this difference may arise from the gap of the spatial extent of the σ orbit between ^{10}Be-^{10}C and ^{14}C-^{14}O.

In addition to 0^+ states, we show the comparison of excitation energies for $J^\pi = 2^+$ and 4^+ states in Figs. 3 and 4, respectively. For 2^+ state, the energy difference of the π-bond linear-chain states is also small ($\Delta E_x = 0.24$ MeV) and the same magnitude as that of the 2^+ member states in the ground band. In contrast, the larger difference of the σ-bond linear-chain states ($\Delta E_x = 1.31$ MeV) can be also seen clearly. It is close to the Coulomb energy difference, 1.04 MeV in Table II. The same tendency as the 0^+ states appears in the 2^+ states, i.e., the energy shift is negligibly small for the π-bond linear-chain states, while it is prominent for the σ-bond linear-chain states because of the Coulomb energy reduction. For 4^+ state, π- and σ-bond linear-chain states of ^{14}O are fragmented into two states due to the coupling with other configuration. The lower σ-bond linear-chain state shows the large energy shift, 1.49 MeV. However, it cannot be explained as the Coulomb energy reduction because the Coulomb energy difference is 0.34 MeV, which is too small. It shows that the mirror system does not have the good charge symmetry written by Eq. (12) for 4^+ state.

Finally, we predict the α-decay widths of the linear-chain states in ^{14}O and ^{14}C. Calculated widths for several decay channels are listed in Table IV. In order to compare with ^{14}C, calculated widths of ^{14}C are also listed in Table V. The channel radii a are 5.00 fm for the π-bond linear chain and 6.50 fm for the σ-bond linear chain, which are chosen to be smoothly connected to the Coulomb wave function. The π-bond linear-chain states have rather large α-decay widths which decay into the ground state of the daughter nucleus. While the threshold of $\alpha + ^{10}$C is 1.79 MeV lower than that of $\alpha + ^{10}$Be, the excitation energies of the π-bond linear-chain states are almost the same in ^{14}O and ^{14}C. As the result, α-decay widths of the π-bond linear chain in ^{14}O are larger than those in ^{14}C except for the 4^+ state. For the decay into the first excited state, namely, ^{10}C(2^+_1) and ^{10}Be(2^+_1), the decay widths are larger than those of decay into the ground states. We consider that it is due to the strong coupling of

TABLE IV. Excitation energies (MeV) and α-decay widths (keV) of the linear-chain states in ^{14}O. The channel radii are $a = 5.00$ and 6.50 fm for π-bond and σ-bond linear chains, respectively.

Linear chain	J^π	E_x	$\Gamma_\alpha(^{10}\mathrm{C}(0^+_1))$	$\Gamma_\alpha(^{10}\mathrm{C}(2^+_1))$	$\Gamma_\alpha(^{10}\mathrm{C}(0^+_2))$	$\Gamma_\alpha(^{10}\mathrm{C}(2^+_3))$
π bond	0^+	14.37	1.15×10^3	1.55×10^3	0.04	
	2^+	15.74	1.22×10^3	1.99×10^3	2.24	0.00
	4^+	17.36	4.12×10^2	1.04×10^3	1.43	0.49
	4^+	18.13	6.32×10^2	1.42×10^3	3.34	2.31
σ bond	0^+	20.45	6.30	19.0	7.68×10^2	1.95×10^3
	2^+	21.36	4.75	11.8	6.29×10^2	1.73×10^3
	4^+	22.67	4.97	16.8	3.09×10^2	9.39×10^2
	4^+	23.15	3.21	7.50	3.54×10^2	1.08×10^3

TABLE V. Excitation energies (MeV) and α-decay widths (keV) of the linear-chain states in ^{14}C. The channel radii are $a = 5.00$ and 6.50 fm for π-bond and σ-bond linear chains, respectively.

Linear chain	J^π	E_x	$\Gamma_\alpha(^{10}\mathrm{Be}(0_1^+))$	$\Gamma_\alpha(^{10}\mathrm{Be}(2_1^+))$	$\Gamma_\alpha(^{10}\mathrm{Be}(0_2^+))$	$\Gamma_\alpha(^{10}\mathrm{Be}(2_3^+))$
π bond	0^+	14.45	1.37×10^3	1.02×10^3		
	2^+	15.98	1.29×10^3	1.84×10^3	0.63	
	4^+	18.40	1.10×10^3	2.29×10^3	3.88	2.77
σ bond	0^+	21.98	1.34	0.86	7.69×10^2	2.20×10^3
	2^+	22.67	2.78	5.71	7.72×10^2	2.30×10^3
	4^+	24.16	1.20	1.73	7.73×10^2	2.47×10^3

the linear-chain configuration; therefore, this can be a good signature for identifying the linear chain in observation.

In contrast to the π-bond linear chain, smaller decay widths into the $^{10}\mathrm{C}(0_1^+, 2_1^+)$ are shown for the σ-bond linear chain. Alternatively, the σ-bond linear-chain states show the large α-decay widths which decay into the 0_2^+ and 2_3^+ states of ^{10}C. As mentioned previously, our calculation shows that the valence protons of the ground state and 2_1^+ state in ^{10}C occupy the π orbit, while those of the 0_2^+ and 2_3^+ states in ^{10}C occupy the σ orbit. Thus, this result can be interpreted as the molecular-orbital picture. Also, these characteristic patterns of the α-decay widths are the same as ^{14}C. However, in contrast to the the π-bond linear chain, the decay widths of ^{14}C are larger than those of ^{14}O in the case of the σ-bond linear chain. It may be affected by the reduction of the excitation energy of the σ-bond linear-chain state in ^{14}O due to the Thomas-Ehrman shift.

Summary. We discussed the energy shift of the linear-chain states in ^{14}C-^{14}O based on the AMD calculation. In ^{14}O, we find three types of cluster configuration: the triangular, π-bond linear chain, and σ-bond linear chain. These same configurations are already found in ^{14}C. The energy shift is negligibly small for the π-bond linear chain while it is prominent for the σ-bond linear chain. The large energy difference of the σ-bond linear chain can be accounted for in terms of the reduction in the Coulomb energy associated with the spatial extent of the σ orbit. This result is supported by the large radius of the single-particle orbit and the reduction of the Coulomb energy of the σ orbit. Therefore, the Thomas-Ehrman shift can bee seen clearly in the σ-bond linear chain. The same character is also seen in the mirror pair of ^{10}Be-^{10}C. Moreover, we predict the α-decay widths of the linear-chain states in ^{14}O to compare with observations which will be reported in future. The π-bond linear-chain states show large α-decay widths into the $^{10}\mathrm{C}(0_1^+, 2_1^+; \pi^2)$ whereas the σ-bond linear-chain states show large α-decay widths into the $^{10}\mathrm{C}(0_2^+, 2_3^+; \sigma^2)$. Both linear chains show that the α-decay widths into the 2^+ state of ^{10}C are larger than those of the 0^+ state. These decay patterns are qualitatively the same for ^{14}C. The Thomas-Ehrman shift, large α-decay widths, and characteristic decay patterns can be good signatures of the linear-chain structures in ^{14}O and ^{14}C, if they is observed.

Acknowledgments. T.B. acknowledges support by JSPS KAKENHI Grant No. JP16J04889. M.K. acknowledges the support of the Grants-in-Aid for Scientific Research on Innovative Areas from MEXT (Grant No. 2404:24105008) and JSPS KAKENHI Grant No. JP16K05339.

[1] H. Morinaga, Phys. Rev. **101**, 254 (1956).
[2] N. Itagaki, S. Okabe, K. Ikeda, and I. Tanihata, Phys. Rev. C **64**, 014301 (2001).
[3] B. J. Greenhalgh, B. R. Fulton, D. L. Watson, N. M. Clarke, L. Donadille, M. Freer, P. J. Leask, W. N. Catford, K. L. Jones, and D. Mahboub, Phys. Rev. C **66**, 027302 (2002).
[4] H. G. Bohlen, R. Kalpakchieva, B. Gebauer, S. M. Grimes, H. Lenske, K. P. Lieb, T. N. Massey, M. Milin, W. von Oertzen, Ch. Schulz, T. Kokalova, S. Torilov, and S. Thummerer, Phys. Rev. C **68**, 054606 (2003).
[5] N. I. Ashwood, M. Freer, J. C. Angelique, V. Bouchat, W. N. Catford, N. M. Clarke, N. Curtis, O. Dorvaux, F. Hanappe, Y. Kerckx, M. Labiche, J. L. Lecouey, F. M. Marques, T. Materna, A. Ninane, G. Normand, N. A. Orr, S. Pain, N. Soic, L. Stuttge, C. Timis, A. Unshakova, and V. A. Ziman, Phys. Rev. C **70**, 064607 (2004).
[6] J. Maruhn, N. Loebl, N. Itagaki, and M. Kimura, Nucl. Phys. A **833**, 1 (2010).
[7] T. Suhara and Y. Kanada-En'yo, Phys. Rev. C **82**, 044301 (2010).
[8] T. Suhara and Y. Kanada-En'yo, Phys. Rev. C **84**, 024328 (2011).
[9] M. Freer, J. D. Malcolm, N. L. Achouri, N. I. Ashwood, D. W. Bardayan, S. M. Brown, W. N. Catford, K. A. Chipps, J. Cizewski, N. Curtis, K. L. Jones, T. Munoz-Britton, S. D. Pain, N. Soic, C. Wheldon, G. L. Wilson, and V. A. Ziman, Phys. Rev. C **90**, 054324 (2014).
[10] J.-P. Ebran, E. Khan, T. Niksic, and D. Vretenar, Phys. Rev. C **90**, 054329 (2014).
[11] T. Baba, Y. Chiba, and M. Kimura, Phys. Rev. C **90**, 064319 (2014).
[12] P. W. Zhao, N. Itagaki, and J. Meng, Phys. Lett. **115**, 022501 (2015).
[13] A. Fritsch, S. Beceiro-Novo, D. Suzuki, W. Mittig, J.J. Kolata, T. Ahn, D. Bazin, F. D. Becchetti, B. Bucher, Z. Chajecki, X. Fang, M. Febbraro, A. M. Howard, Y. Kanada-En'yo, W. G. Lynch, A. J. Mitchell, M. Ojaruega, A. M. Rogers, A. Shore, T. Suhara, X. D. Tang, R. Torres-Isea, and H. Wang, Phys. Rev. C **93**, 014321 (2016).
[14] Z. Y. Tian, Y. L. Ye, Z. H. Li, C. J. Lin, Q. T. Li, Y. C. Ge, J. L. Lou, W. Jiang, J. Li, Z. H. Yang, J. Feng, P. J. Li, J. Chen,

Q. Liu, H. L. Zang, B. Yang, Y. Zhang, Z. Q. Chen, Y. Liu, X. H. Sun, J. Ma, H. M. Jia, X. X. Xu, L. Yan, N. R. Ma, and L. J. Sun, Chin. Phys. C **40**, 111001 (2016).
[15] Y. Yoshida and Y. Kanada-En'yo, Prog. Theor. Exp. Phys. **2016**, 123D04 (2016).
[16] T. Baba and M. Kimura, Phys. Rev. C **94**, 044303 (2016).
[17] H. Yamaguchi, D. Kahl, S. Hayakawa, Y. Sakaguchi, K. Abe, T. Nakao, T. Suhara, N. Iwasa, A. Kim, D. H. Kim, S. M. Cha, M. S. Kwag, J. H. Lee, E. J. Lee, K. Y. Chae, Y. Wakabayashi, N. Imai, N. Kitamura, P. Lee, J. Y. Moon, K. B. Lee, C. Akers, H. S. Jung, N. N. Duy, L. H. Khiem, and C. S. Lee, Phys. Lett. B **766**, 11 (2017).
[18] J. Li, Y. L. Ye, Z. H. Li, C. J. Lin, Q. T. Li, Y. C. Ge, J. L. Lou, Z. Y. Tian, W. Jiang, Z. H. Yang, J. Feng, P. J. Li, J. Chen, Q. Liu, H. L. Zang, B. Yang, Y. Zhang, Z. Q. Chen, Y. Liu, X. H. Sun, J. Ma, H. M. Jia, X. X. Xu, L. Yang, N. R. Ma, and L. J. Sun, Phys. Rev. C **95**, 021303(R) (2017).
[19] T. Baba and M. Kimura, Phys. Rev. C **95**, 064318 (2017).
[20] J.-P. Ebran, E. Khan, T. Niksic, and D. Vretenar, J. Phys. G **44**, 103001 (2017).
[21] T. Baba and M. Kimura, Phys. Rev. C **97**, 054315 (2018).
[22] M. Seya, M. Kohno, and S. Nagata, Prog. Theor. Phys. **65**, 204 (1981).
[23] W. von Oertzen, Z. Phys. A **354**, 37 (1996); **357**, 355 (1997).
[24] N. Itagaki and S. Okabe, Phys. Rev. C **61**, 044306 (2000).
[25] R. G. Thomas, Phys. Rev. **88**, 1109 (1952).
[26] J. B. Ehrman, Phys. Rev. **81**, 412 (1951).
[27] L. V. Grigorenko, I. G. Mukha, I. J. Thompson, and M. V. Zhukov, Phys. Rev. Lett. **88**, 042502 (2002).
[28] E. Garrido, D. V. Fedorov, and A. S. Jensen, Phys. Rev. C **69**, 024002 (2004).
[29] L. V. Grigorenko, T. A. Golubkova, and M.V. Zhukov, Phys. Rev. C **91**, 024325 (2015).
[30] M. Nakao, H. Umehara, S. Ebata, and M. Ito, Phys. Rev. C **98**, 054318 (2018).
[31] M. Ito, EPJ. Conf. **117**, 06014 (2016).
[32] J. F. Berger, M. Girod, and D. Gogny, Comput. Phys. Comm. **63**, 365 (1991).
[33] M. Kimura, Phys. Rev. C **69**, 044319 (2004).
[34] Y. Kanada-En'yo and H. Horiuchi, Prog. Theor. Phys. **93**, 115 (1995).
[35] D. L. Hill and J. A. Wheeler, Phys. Rev. **89**, 1102 (1953).
[36] Y. Chiba and M. Kimura, Prog. Theor. Exp. Phys. **2017**, 053D01 (2017).
[37] A. Volkov, Nucl. Phys. **74**, 33 (1965).